Efficient Synthesis of Concentric-Rings Plane Wave Generators

D. Pinchera, *Senior Member, IEEE*, M. D. Migliore, *Senior Member, IEEE*

***Abstract*—In this paper, we present an efficient method for synthesizing sparse plane wave generators (PWGs) based concentric ring arrays. In particular, we introduce a novel circularly-polarized ring source whose field on a near-field surface can be represented using only three scalar functions. Using this representation, we can simplify the synthesis, reducing substantially its computational complexity, which can be easily handled using an ordinary office PC. After using the ring sources to identify the position and excitation of the PWG elements, we can employ discrete linearly polarized sources as feeds or use different kinds of radiators. Some numerical simulations validate the proposed approach, which can obtain planar and volumetric quiet zones with good polarization purity.**

***Index Terms*—Antenna arrays, Antenna radiation pattern synthesis, Optimization methods, Sparse array antennas**

I. Introduction

The widespread diffusion of always more complex communication technology requires sophisticated test equipment to characterize radiating systems correctly.

In particular, the proper validation of 5G and forthcoming 6G communication systems requires testing the terminals and base station antennas in conditions very close to the working ones. Unfortunately, the classical far-field testing of radiating equipment may require huge anechoic chambers. It is also possible to employ compact-range test sites, but these systems are expensive and large and show limited flexibility in the realization of measurements [1].

A possibility proposed in the last decades is using a Plane Wave Generator (PWG) [2]. It consists of an antenna array able to synthesize a plane wave, or a superposition of plane waves, in a desired region of space, usually referred to as Quiet Zone (QZ). The size of the PWG is generally slightly larger than the dimension of the QZ to realize; the performance achievable by PWGs, as well as their design guidelines and some useful rules-of-thumb for their dimensioning and synthesis, are discussed in [3].

The advantage of a PWG with respect to concurrent solutions is its compactness. It is also possible to perform complex tests on antennas: 5G base station testing [4]; ultrawideband systems [5]; 5G NR testing [6]; measurements in small anechoic chambers [7]; emulation of multipath environment [8]. The main disadvantage is their cost, mainly related to the synthesis of the beamforming network and the number of amplifiers/attenuators and phase shifters needed for providing the correct excitation to the radiators. For this reason, reducing the number of radiators is one of the critical points in designing this kind of system. Aperiodic architectures are particularly advantageous from this point of view: non-regular grids [3], circular rings [9], sparse arrays [10].

From an engineering perspective, the design of a PWG shares many points with the problem of antenna array synthesis. Still, it is generally more complex to handle from a numerical point of view. Even if the single radiators constituting the PWG work in far-field conditions, the overall PWG does not work in the same condition: we cannot exploit the factorization of the radiated field into element factor and array factor [3]. Moreover, the design of sparse PWGs is challenging due to the nonlinearity of the radiated field with respect to the radiators' position variables.

Moreover, suppose we require excellent polarization purity. In that case, the number of equations involved in the synthesis is tripled since the request for a quiet zone with a vertically polarized field in a specific direction requires that we appropriately limit the amplitude of the other two electromagnetic field components.

This paper proposes an approach for synthesizing PWGs arranged into rings. In particular, we take advantage of the fact that we can realize linear polarization as the summation of two circular polarizations. To this aim, we introduce a very convenient representation of the radiated field that exploits the symmetries of circularly polarized ring sources. This way, we can represent the fields radiated on a surface using only three scalar functions of a single spatial variable: the synthesis's computational complexity becomes similar to sparse linear array synthesis. We must underline that the proposed circularly polarized source is only employed as a synthesis tool since we substitute it with simpler linearly polarized feeds in the final design. The synthesized PWG will radiate a plane wave with excellent uniformity and polarization purity within the QZ.

The paper is organized in the following way. We first discuss the field radiated by a circularly polarized ring source (section II). Then we use the introduced representation to synthesize the PWG (section III). More precisely, the synthesis is split into two steps: we will first identify a set of concentric ring sources, then we will find the correct number of elementary sources per ring to radiate the desired field. Examples of PWGs employing simple linearly polarized sources will confirm the effectiveness of the proposed procedure (section IV). Conclusions follow.

Manuscript received on ····.

Daniele Pinchera and Marco Donald Migliore are with DIEI (Departement of Electrical and Information Engineering) - University of Cassino and Southern Lazio, CNIT (Italian National Consortium for Telecommunications) and ELEDIA@UniCAS, via G. Di Biasio 43, 03043 Cassino, Italy e-mail: pinchera@unicas.it, mdmiglio@unicas.it

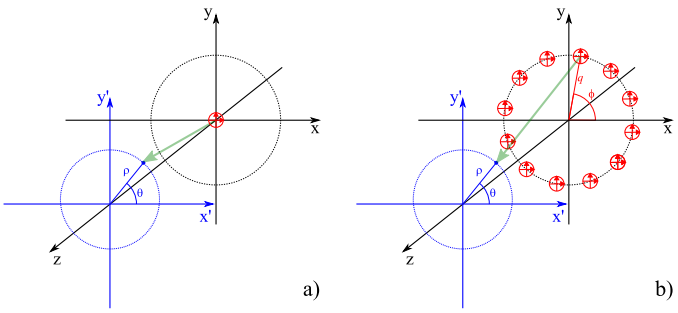

Fig. 1. Scheme of the system: the sources are placed on (x, y) plane (black), the observation region is the (x', y') plane (blue). Subplot a): we have a single CPES (red) in the origin of axis. Subplot b): we have a CPCRS of radius q (only 12 CPES are displayed for simplicity).

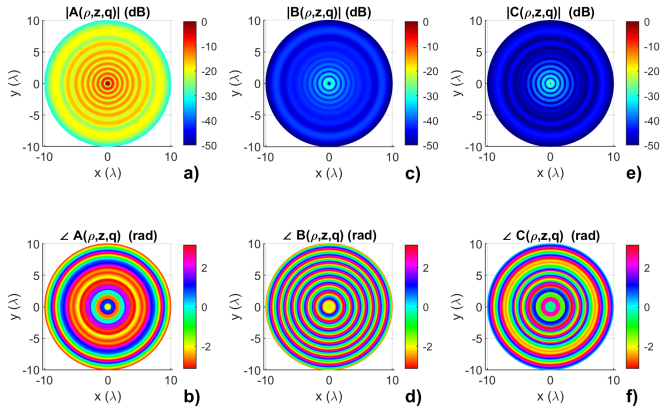

Fig. 2. Amplitude (a,c,e) and phase (b,d,f) of the functions $A(\rho, z, q)$, $B(\rho, z, q)$ and $C(\rho, z, q)$ relative to RH-CPCRS of radius $q = 5\lambda$ evaluated on a circular area of maximum radius $\rho = 10\lambda$ for a distance $z = 5\lambda$ from the source's plane. The amplitudes have been normalized to the maximum amplitude of $A(\rho, z, q)$.

II. Introducing a Symmetrical Source

The free space wavelength and the corresponding wavenumber will be indicated in the following section with λ and β, respectively. To simplify the notation, when calculating the field of elementary sources, we will suppose that the distance of the observation point from the single elementary source is always sufficiently large to use the far-field representation for the radiation of each source [11]. Normal fonts will be used to represent scalar quantities, and bold fonts will be used to describe vector quantities.

To simplify the synthesis of the PWG, we will now introduce a Circularly Polarized Elementary Source (CPES), which is the superposition of two coherent orthogonal elementary sources of equal amplitude having a phase shift of $\pi/2$. Suppose that the two orthogonal directions of the CPES are parallel to x and y axes; we will refer to Right-Handed-CPES if the current of the elementary source is proportional to the complex vector $\mathbf{i}_r = (\mathbf{i}_y + j\mathbf{i}_x)$, and of Left-Handed-CPES if the current of the elementary source is proportional to the complex vector $\mathbf{i}_\ell = (\mathbf{i}_y - j\mathbf{i}_x)$.

With reference to Fig.1a, let us consider an RH-CPES placed in the origin of axes; its radiative field [11] in a point of polar coordinates (ρ, θ, z) belonging to the observation plane (x', y') can be calculated as:

$$\tilde{\mathbf{E}_\mathbf{0}}^{(r)}(\rho, \theta, z) = \frac{\alpha I}{\lambda R_0} e^{-j\beta R_0}(((\mathbf{i}_y + j\mathbf{i}_x) \times \mathbf{i}_{R_0}) \times \mathbf{i}_{R_0}) \quad (1)$$

where $(\mathbf{i}_x, \mathbf{i}_y, \mathbf{i}_z)$ are the real Cartesian versors, α is an inessential constant, I is a complex amplitude factor, $\mathbf{R_0} = \rho\cos\theta\mathbf{i}_x + \rho\sin\theta\mathbf{i}_y + z\mathbf{i}_z$, $R_0 = |\mathbf{R_0}|$ and $\mathbf{i}_{R_0} = \mathbf{R_0}/R_0$

With minor algebra calculations discussed in the appendix, it turns out to be particularly convenient to represent this field with respect to the three vectors $(\mathbf{i}_r, \mathbf{i}_\ell, \mathbf{i}_z)$:

$$\tilde{\mathbf{E}_\mathbf{0}}^{(r)}(\rho, \theta, z) = A_0(\rho, z)\mathbf{i}_r + B_0(\rho, z)e^{-j2\theta}\mathbf{i}_\ell + C_0(\rho, z)e^{-j\theta}\mathbf{i}_z \quad (2)$$

where $A_0(\rho, z)$, $B_0(\rho, z)$ and $C_0(\rho, z)$ are three complex scalar functions independent from θ, providing, respectively, the complex amplitude of the right-handed, left-handed and z-component of the field.

This very convenient formulation is also possessed by a continuous distribution of equal-amplitude CPES along a ring; we will refer to it in the following as Circularly Polarized Continuous Ring Source (CPCRS).

In particular, with reference to fig.1b, let us evaluate the radiative field of a Right-Handed CPCRS of radius q centered in the origin of axes:

$$\mathbf{E}^{(r)}(\rho, \theta, z, q) = \int_0^{2\pi} \tilde{\mathbf{E}}^{(r)}(\rho, \theta, z, q, \phi) q d\phi \quad (3)$$

where $\tilde{\mathbf{E}}^{(r)}(\rho, \theta, z, q, \phi)$ is the field radiated in the point (ρ, θ, z) by the RH-CPES located in $(q, \phi, 0)$:

$$\tilde{\mathbf{E}}^{(r)}(\rho, \theta, z, q, \phi) = \frac{\alpha I}{\lambda R} e^{-j\beta R}(((\mathbf{i}_y + j\mathbf{i}_x) \times \mathbf{i}_R) \times \mathbf{i}_R) \quad (4)$$

where

$$\mathbf{R} = (\rho\cos\theta - q\cos\phi)\mathbf{i}_x + (\rho\sin\theta - q\sin\phi)\mathbf{i}_y + z\mathbf{i}_z \quad (5)$$

with $R = |\mathbf{R}|$ and $\mathbf{i}_R = \mathbf{R}/R$.

In the appendix, we demonstrate that we can write the field radiated by the RH-CPCRS as:

$$\begin{aligned}\mathbf{E}^{(r)}(\rho, \theta, z, q) = & A(\rho, z, q)\mathbf{i}_r + B(\rho, z, q)e^{-j2\theta}\mathbf{i}_\ell \\ & + C(\rho, z, q)e^{-j\theta}\mathbf{i}_z \end{aligned} \quad (6)$$

and the field radiated by the LH-CPCRS as:

$$\begin{aligned}\mathbf{E}^{(\ell)}(\rho, \theta, z, q) = & A(\rho, z, q)\mathbf{i}_\ell + B(\rho, z, q)e^{+j2\theta}\mathbf{i}_r \\ & + C(\rho, z, q)e^{+j\theta}\mathbf{i}_z \end{aligned} \quad (7)$$

where $A(\rho, z, q)$, $B(\rho, z, q)$ and $C(\rho, z, q)$ are proper scalar functions, independent from θ, that can be evaluated by means of numerical integration. In Fig.2, it is possible to see their behavior for an RH-CPCRS of radius $q = 5\lambda$ evaluated on an observation plane with $z = 5\lambda$.

It is worth noting that the amplitude of $A(\rho, z, q)$ is stronger than the amplitude of the other two functions, confirming the intuitive result that a circularly polarized source radiates a field prevalently polarized in the same way. Unfortunately, the field radiated by a single ring presents a significant cross-polar and z-component, and the field is not sufficiently uniform in amplitude to generate a plane wave. Still, a proper combination of rings may be suitable to solve the mentioned task, and this approach will be exploited in the next section.

III. Synthesis method

This section will show how we can exploit the circularly polarized source introduced in the previous section to synthesize a PWG. Two sequential steps are involved: first, we will find a proper set of rings to synthesize the plane wave; second, we will substitute the continuous rings with discrete sources.

Let us focus on the objective of synthesizing a right-handed circularly polarized plane wave in a circular region of the (x', y') plane (see Fig.1) employing N concentric rings. We can translate this problem into finding an optimal value of the number of rings N, the radii q_n and the complex amplitudes I_n for the N rings so that for $\rho < \rho_{MAX}$ we have:

$$\left|\left(\sum_{n=1}^{N} I_n A(\rho, z, q_n)\right) - 1\right| < \epsilon_A \tag{8}$$

$$\left|\sum_{n=1}^{N} I_n B(\rho, z, q_n)\right| < \epsilon_B \tag{9}$$

$$\left|\sum_{n=1}^{N} I_n C(\rho, z, q_n)\right| < \epsilon_C \tag{10}$$

where ρ_{MAX} is the radius of the region in which we want to synthesize the plane wave, $(A(\rho, z, q_n); B(\rho, z, q_n); C(\rho, z, q_n))$ are the functions introduced in (6) for the $n-$th ring of radius q_n, and $(\epsilon_A, \epsilon_B, \epsilon_C)$ are suitable approximation thresholds. It is worth underlining that the dependence from the θ parameter can be neglected so that we can deal with a single spatial variable.

A. Finding the continuous rings

We can follow several approaches for finding the number of rings, their radii, and excitations; since we would like to reduce the complexity of the PWG, we will aim to minimize the number of rings. This task shares many similarities with the sparse array synthesis problem, so we can follow a compressive sensing inspired approach [12], using the smooth-reweighted ℓ_1 minimization introduced in [13].

To this aim, we will consider a set of ν closely spaced rings of radii $(q_1, \cdots, q_\nu)$, and we will collect their excitations in the column vector $\mathcal{I} = [I_1, \cdots, I_\nu]$. We will also define a proper set of μ points $(\rho_1, \cdots, \rho_\mu)$ sampling the radius of the circular area of diameter $2\rho_{MAX}$ in which we would like to synthesize the plane wave. We will also introduce three complex valued $(\mu \times \nu)$ matrices $(\mathcal{A}, \mathcal{B}, \mathcal{C})$, so that the m, n elements of these matrices are

$$\mathcal{A}_{m,n} = A(\rho_m, z, q_n) \tag{11}$$

$$\mathcal{B}_{m,n} = B(\rho_m, z, q_n) \tag{12}$$

$$\mathcal{C}_{m,n} = C(\rho_m, z, q_n). \tag{13}$$

We can then solve the following smooth-weighted convex problem iteratively:

$$minimize \qquad \|\mathcal{W} \circ \mathcal{I}\|_1 \tag{14}$$

$$subject\ to \qquad |\mathcal{A}\mathcal{I} - 1|_\infty \leq \epsilon_a \tag{15}$$

$$|\mathcal{B}\mathcal{I}|_\infty \leq \epsilon_b \tag{16}$$

$$|\mathcal{C}\mathcal{I}|_\infty \leq \epsilon_c \tag{17}$$

where $\mathcal{W} = [w_1, \cdots, w_\nu]$ is the smooth weighting vector defined in the following, $\mathcal{W} \circ \mathcal{I}$ is the Hadamard entrywise product of the two vectors $\mathcal{W}$ and $\mathcal{I}$, $\|\cdot\|_1$ is the ℓ_1 norm of a vector.

As shown in [13], when the weighted minimization problem (14)-(17) is solved, the excitation vector $\mathcal{I}$ will show some "clusters" of non-null values. Differently from the standard re-weighted ℓ_1 norm minimization [12], we can preserve the information content of the clusters using a "smooth" weighting vector. In particular, we have used:

$$w_n = 1/\max(g_n, \eta) \tag{18}$$

where η is a small positive threshold to prevent too large values for w_n, and g_n are the entries of the vector $\mathcal{G}$ calculated as

$$\mathcal{G} = |\mathcal{I}'| * \mathcal{D} \tag{19}$$

where $\mathcal{I}'$ is the excitation vector obtained in the previous iteration, the convolution "$*$" returns only the central part of it (of the same size as $\mathcal{I}$), and $\mathcal{D}$ is a smoothing vector of positive numbers. For instance, in the numerical examples of this paper, we have used $\mathcal{D} = [.25; .5; .99; 1; .99; .5; .25]$.

The convergence of the proposed method is fast; usually, after about ten iterations, we can observe no more changes in $\mathcal{I}$. After the convergence, we can extract the ring radii q_n, and excitations I_n through a weighted average of the clusters of non-null value that appear in the excitation vector $\mathcal{I}$ [13].

We must underline that in this approach, the number N of the found CPCRSs is one of the synthesis outputs, so it can not be determined a-priori. Still, it is possible to repeat the synthesis with different values of the thresholds $(\epsilon_A, \epsilon_B, \epsilon_C)$ until we achieve the desired result - higher thresholds usually result in a lower number of rings, with a larger spacing between them, to satisfy the synthesis.

The use of higher thresholds $(\epsilon_A, \epsilon_B, \epsilon_C)$ is also a good workaround to the lack of an explicit constraint on the distance between the rings. In this way, we accept a lower accuracy for the generated plane wave, but we can avoid overlapping radiators.

Another possible workaround to the ring-spacing issue may be using a different synthesis algorithm for identifying the CPCRSs, like I-IDEA [14], that allows us to take into account the spacing constraint explicitly.

Moreover, we may add, if needed, further convex constraints in the problem defined in (14)-(17); for instance, we may limit the maximum amplitude of the field in specific regions outside the QZ. It may also be possible to build a convex constraint to limit the integral of the power flux in regions out of the QZ to maximize the power efficiency of the PWG. Since we found that the achieved field levels were satisfactory, we did not follow those approaches in the examples of the present paper.

As a final observation, we have to underline that, in some cases, the constraint (17) on the z-component in the convex problem is automatically satisfied because of the relative weakness of such a field component. In our numerical tests, we chose to leave that constraint in the convex problem since it allowed us to maintain the z-component always under control without significantly influencing the algorithm's convergence.

This article has been accepted for publication in IEEE Transactions on Antennas and Propagation. This is the author's version which has not been fully edited and content may change prior to final publication. Citation information: DOI 10.1109/TAP.2023.3263011

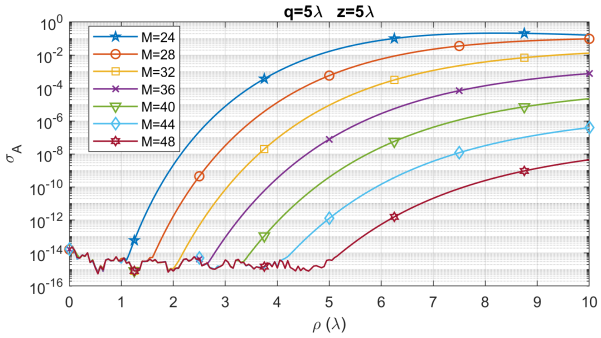

Fig. 3. Standard deviation of the circularly polarized right-handed component of the field $A_M(\rho,\theta,z,q)$ along an observation circle of variable radius ρ, for a discrete source of M angularly equispaced circularly polarized elements of radius $q=\lambda$ at a distance $z=5\lambda$ from the source plane. To provide a fair comparison between different values of M, $A_M(\rho,\theta,z,q)$ has been normalized to its maximum value before calculating the standard deviation.

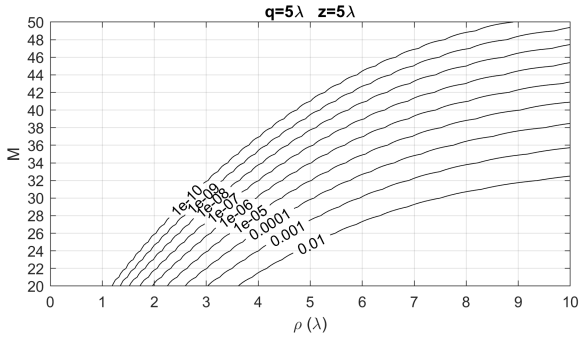

Fig. 4. The relationship between the observation angle ρ, the number of discrete sources M for some values of σ_A (the values on the curves) for a CPDRS of radius $q=\lambda$ at a distance $z=5\lambda$ from the source plane. To provide a fair comparison between different values of M, $A_M(\rho,\theta,z,q)$ has been normalized to its maximum value before calculating the standard deviation.

B. Continuous ring discretization

Once we have found the ring radii, we can substitute the continuous rings with a proper set of discrete circularly polarized sources.

The fact that we pass from a continuous distribution of sources to an angularly-equispaced Circularly Polarized Discrete Ring Source (CPDRS) of M CP sources of equal amplitude will result in a slightly more complex field. For instance, for an RH-CPDRS, we will have:

$$\tilde{\mathbf{E}}^{(r)}(\rho,\theta,z,q)=A_M(\rho,\theta,z,q)\mathbf{i}_r+B_M(\rho,\theta,z,q)e^{-j2\theta}\mathbf{i}_\ell +C_M(\rho,\theta,z,q)e^{-j\theta}\mathbf{i}_z \quad (20)$$

where the scalar functions (A_M,B_M,C_M) will show some oscillations with respect of the variable θ with the same periodicity of the angular spacing between the discrete sources.

It turns out that the amplitude of these oscillations along the observation ring shows a behavior very similar to the phenomena of pseudo-grating lobes for ring arrays [15]. In Fig.3, we analyze the case of a CPDRS of radius $q=5\lambda$ and a variable number M of angularly-equispaced CPES. Apart from some minor ripples, the standard deviation σ_A of the circularly polarized field component $A_M(\rho,\theta,z,q)$ shows an increasing behavior with respect to the increase of ρ and a decreasing behavior with respect to the increase of M.

It is relatively easy to numerically calculate the relationship between the coordinate of the observation point ρ and the number of discrete sources M. Again, with reference to the same CPDRS of radius $q=5\lambda$, in Fig.4, we provide a plot of the relationship between ρ and M for some values of σ_A.

Using these curves, we can find the number of discrete sources M_n (with $n\in[1,N]$) for each of the N rings that achieves the desired approximation level up to ρ_{MAX}; as an example, looking at Fig.4 we can determine that for a source ring of radius $q=\lambda$ at a distance $z=5\lambda$ from the source plane we need at least $M=34$ discrete sources to obtain a value of $\sigma_A<0.001$ for an observation region within $\rho<=8\lambda$. In this paper, we have chosen to consider as design criteria a value of σ_A at least two orders of magnitude lower than the smallest between the thresholds ϵ_A, ϵ_B, and ϵ_C.

C. Achieving a linear polarization

The procedure described before allows the synthesis of the parameters (q_n,I_n,M_n) for the set of CPDRS relative to the PWG that generates an RH circularly polarized plane wave of unit amplitude. The field radiated by this RH-PWG in the circular QZ area can be written as:

$$\mathbf{E}^{(r)}_{PWG}(\rho,\theta)=(\mathbf{i}_y+j\mathbf{i}_x)+\mathbf{err}^{(r)}(\rho,\theta) \quad (21)$$

wherein the term $\mathbf{err}^{(r)}(\rho,\theta)$ is an error term whose magnitude depends on the choice of the thresholds ϵ_A,ϵ_B,ϵ_C, and σ_A.

Obviously, because of the symmetry, if instead of RH sources, we used LH sources with the same radiators' layout, the resulting LH-PWG radiates a field:

$$\mathbf{E}^{(\ell)}_{PWG}(\rho,\theta)=(\mathbf{i}_y-j\mathbf{i}_x)+\mathbf{err}^{(\ell)}(\rho,\theta) \quad (22)$$

wherein the term $\mathbf{err}^{(\ell)}(\rho,\theta)$ is, again, an error term whose magnitude depends on the choice of the thresholds ϵ_A,ϵ_B,ϵ_C, and σ_A.

It is then possible to exploit the linearity of the fields to obtain the field of a linearly polarized plane wave. Remembering that $\mathbf{i}_y=(\mathbf{i}_r+\mathbf{i}_\ell)/2$, we can substitute the CPES of the RH-PGW and the LH-PWG with $\mathbf{i}_y$ elementary sources, obtaining the field of the $\mathbf{y}-$PWG as:

$$\mathbf{E}^{(y)}_{PWG}(\rho,\theta)=(\mathbf{i}_y)+(\mathbf{err}^{(r)}(\rho,\theta)+\mathbf{err}^{(\ell)}(\rho,\theta))/2 \quad (23)$$

The last equation shows that the field in the QZ, apart from an error term of controllable amplitude, is linearly polarized. This helpful feature allows us to exploit the circular symmetry of CPCRS to simplify the PWG synthesis and use simple linear polarized elementary sources to achieve a linearly polarized field in the QZ. In the next paragraph, we will use simple linear polarized elementary sources to synthesize linearly polarized quiet zones to show this feature.

IV. Numerical Examples

In this section, we will provide some examples that confirm the effectiveness of the proposed approach. All the simulations have been performed for a single frequency, and all the

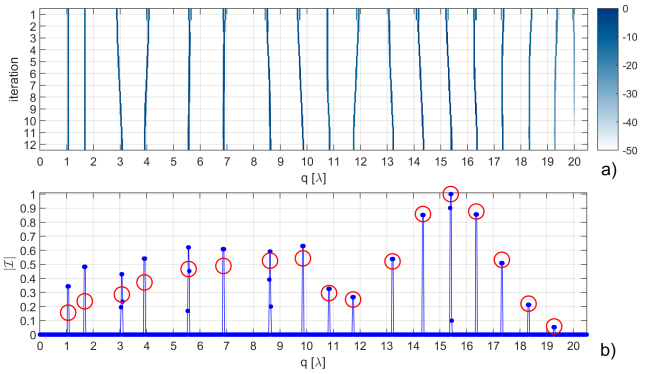

Fig. 5. Graphical representation of the evolution of the solution found for the excitation $\mathcal{I}$ of the dense rings. Subplot a): colormap representing the amplitude in dB of the 12-row matrix collecting the excitation vectors $\mathcal{I}$ for the 12 realized iterations. Subplot b): plot of the amplitude of $\mathcal{I}$ and $\mathbf{I}$ for the last iteration. All the amplitudes in the figure are normalized to the maximum value.

TABLE I
RING RADII (q_n), NUMBER OF ELEMENTS PER RING (M_n) AND RELATIVE EXCITATION I_n FOR THE $N = 17$ RINGS OF THE 662 ELEMENTS PWG.

q_n	M_n	I_n	q_n	M_n	I_n
1.06	8	$0.707e^{-1.221j}$	11.74	44	$1.130e^{-1.591j}$
1.68	12	$1.072e^{-1.894j}$	13.22	48	$2.357e^{-0.856j}$
3.07	16	$1.292e^{-1.205j}$	14.36	50	$3.879e^{-1.226j}$
3.92	20	$1.680e^{-1.856j}$	15.40	54	$4.522e^{-1.801j}$
5.57	26	$2.120e^{-1.368j}$	16.36	56	$3.961e^{-2.532j}$
6.88	30	$2.209e^{-1.824j}$	17.32	58	$2.408e^{3.087j}$
8.63	34	$2.379e^{-1.281j}$	18.32	62	$0.995e^{2.609j}$
9.86	40	$2.454e^{-1.660j}$	19.28	62	$0.263e^{2.147j}$
10.84	42	$1.336e^{-2.167j}$			

distances are expressed in terms of wavelengths relative to that frequency. Moreover, we will use two performance indexes, as suggested in [3], the root mean square error (RMSE) on the QZ region and the maximum amplitude E_{MAX} of the field radiated by the PWG on the plane of the QZ calculated as:

$$E_{MAX} = \max_{z=z_0} ||\mathbf{E}_{PWG}(x, y, z)||_2 \quad \forall (x, y) \qquad (24)$$

where $||\cdot||_2$ is the ℓ_2 norm of the electric field vector and z_0 is the coordinate of the observation plane. It must be noted that values of E_{MAX} up to 20dB will be considered acceptable in this section, since we suppose as in [3] that good quality absorbing panels are employed in the measurement system. Obviously, as stated before, different choices for the synthesis may be done in accordance with the particular specifications of the desired testing system. For the calculations, we have used Matlab and CVX [16] on an Intel i7 8700k office PC, using as synthesis parameters $\eta = 10^{-3}$ and a spacing $\delta_\nu = \lambda/50$ between the dense radii used to discretize the source.

A. Planar QZ Synthesis

In the first example, we will perform a PWG synthesis using the same specifications discussed in [10], where the authors synthesized some planar sparse PWGs able to generate a plane wave in a circular QZ of a radius of $\rho_{MAX} = 17\lambda$ at a distance of $z = 34\lambda$ from the PWG plane. In particular, the "Case 1" PWG employed 1159 radiating elements, placed within a circular area of 20λ maximum radius, and achieved an RMSE of 0.0046 and a value of E_{MAX} greater than 20dB.

By using the proposed ring-synthesis approach, using a set of equispaced rings in the range $(1\lambda; 20\lambda)$ and $\epsilon_A = \epsilon_B = \epsilon_C = 0.005$ we can obtain a set of $N = 17$ rings. The calculation of these rings required 12 iterations in a total time of fewer than five minutes.

To get a better insight into the algorithm, we can look at Fig.5a, where we provide the graphical representation of the evolution of the amplitude of the excitation vector $\mathcal{I}$ in the 12 performed iterations. We can see that the starting solution (iteration 1) presents 18 "clusters", i.e., groups of non-null values for the excitations vector, corresponding to 18 rings. Within a few iterations, the last cluster is gradually reduced in amplitude; the others are slightly moved from their initial solution, obtaining the final set of 17 rings (Fig.5b) and confirming the ring-minimizing behavior of the iterative algorithm defined in (14)-(17).

Once we have calculated the ring radii, we can obtain the number of discrete sources M_n for the $n-$th ring by selecting the lowest number of sources that guarantees $\sigma_A < 10^{-6}$. Once the values of M_n have been calculated with the strategy described in section III.B, we can compute the actual excitation of the radiators belonging to these rings. Since we have imposed small residual oscillations, we can accomplish this task by evaluating the fields only for the ρ variable. All the parameters of the final PWG that account for an overall number of 662 $y-$oriented linearly polarized elementary sources are in table I.

In Fig.6, it is possible to see the plot of the difference between the field radiated by the PWG and the wanted plane wave:

$$\Delta E(x, y, z) = \|\mathbf{E}_{PWG}(x, y, z) - e^{-j\beta z}\mathbf{i}_y\|_2. \qquad (25)$$

It is evident that the difference between the field radiated by the PWG and the desired plane wave is very small in the circle of radius ρ_{MAX}, and the polarization purity is excellent. The achieved RMSE is 0.0045 and a value of $E_{MAX} = 14.6$dB. It is worth mentioning that these performance indexes are better with respect to the layout presented in [10], with a reduction of the radiators of about 43%.

B. Spherical QZ Synthesis

This second example will show how we can extend the proposed procedure to synthesizing "spherical" QZ. A spherical QZ is particularly interesting for measuring systems in which we use the PWG array as the source in a spherical scanning apparatus, like the one described in [4], [17], [18].

The synthesis of a volumetric QZ is generally more numerically complex than the synthesis of a planar one, so the calculations involved may be challenging to handle with ordinary office PCs. Actually, from Fig.6a it is clear that the QZ extends to a larger volume with respect to the planar region used in the synthesis. This behavior is a direct consequence of Huygens' principle and suggests that for the synthesis of a plane wave within a volume, we may impose the wanted

This article has been accepted for publication in IEEE Transactions on Antennas and Propagation. This is the author's version which has not been fully edited and content may change prior to final publication. Citation information: DOI 10.1109/TAP.2023.3263011

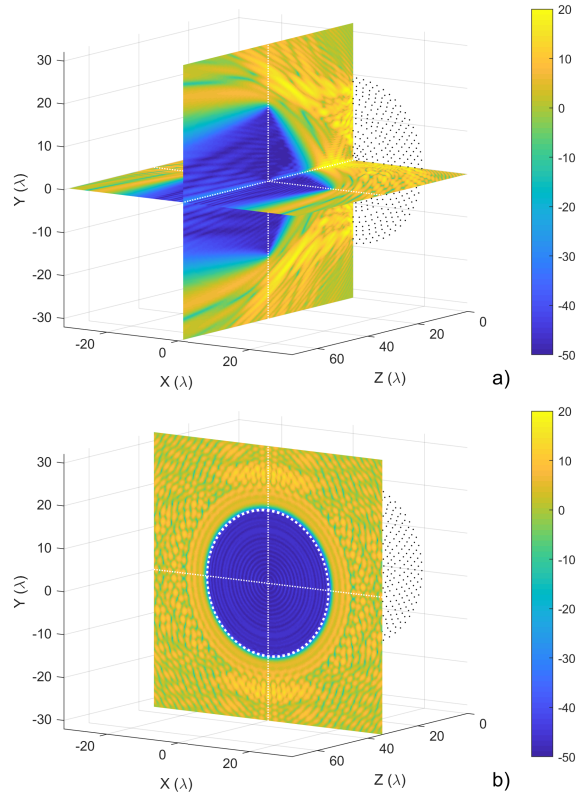

Fig. 6. Difference $\Delta E(x, y, z)$ of the field radiated by the 662 elements PWG and the wanted plane wave: a) the difference is calculated on the $x = 0$ and $y = 0$ planes; b) the difference is calculated on the $z = 34\lambda$ plane. A dashed white line shows the circle of radius ρ_{MAX}.

conditions on the boundary of the desired QZ - in this case, the surface of a sphere.

Now, exploiting again the convenient formulation of the field provided in (6)-(7), we can perform the synthesis imposing the field constraints (15)-(17) on one of the meridian arc of the mentioned spherical surface. This way, we only need to consider a single spatial variable to perform the synthesis.

To show the effectiveness of this approach, we will consider the synthesis of a spherical QZ with specifications similar to the one discussed in [17]. In particular, we will synthesize a plane wave in a sphere of 36λ diameter, with the center at a distance of 112λ from the plane of the PWG. It must be mentioned that the authors of [17] did not explicitly provide the dimension of the employed circular PWG; from the photos of the realized system, we have estimated a size of approximately 42λ diameter at the frequency of 28GHz.

Using the proposed approach and considering a set of densely equispaced rings in the range $(1\lambda; 21\lambda)$ and $\epsilon_A = \epsilon_B = \epsilon_C = 0.01$, we can obtain from the smooth weighted synthesis a set of $N = 9$ rings. The calculation of these rings required 10 iterations in a total time of about ten minutes.

Once the ring radii have been obtained, the number of discrete sources M_n for the $n-$th ring has been calculated by selecting the lowest number of sources that guarantees $\sigma_A < 10^{-4}$. Once the values of M_n have been achieved, it is possible to compute the actual excitation of the radiators. All the parameters of the final PWG, which accounts for an overall number of 170 $y-$oriented linearly polarized elementary sources, are in table II.

TABLE II
RING RADII (q_n), NUMBER OF ELEMENTS PER RING (M_n) AND RELATIVE EXCITATION I_n FOR THE $N = 9$ RINGS OF THE 170 ELEMENTS PWG.

q_n	M_n	I_n	q_n	M_n	I_n
2.16	8	$0.630e^{-2.644j}$	16.24	22	$21.923e^{-1.860j}$
3.48	8	$10.858e^{-1.423j}$	18.26	24	$19.060e^{-2.555j}$
6.92	14	$11.072e^{-1.784j}$	20.02	28	$12.426e^{2.894j}$
10.92	16	$13.538e^{-1.264j}$	21.00	28	$5.096e^{1.134j}$
13.99	22	$16.600e^{-1.245j}$			

TABLE III
RING RADII (q_n), NUMBER OF ELEMENTS PER RING (M_n) AND RELATIVE EXCITATION I_n FOR THE $N = 4$ RINGS OF THE 54 ELEMENTS PWG.

q_n	M_n	I_n	q_n	M_n	I_n
1.03	8	$0.99e^{-1.526j}$	2.84	16	$1.037e^{-2.488j}$
2.124	14	$1.197e^{-1.588j}$	3.52	16	$0.386e^{2.982j}$

In Fig.7, it is possible to see the plot of the difference of $\Delta E(x, y, z)$ (25). The difference between the field radiated by the PWG and the desired plane wave is minimal within the sphere of radius ρ_{MAX}, and we also have an excellent polarization purity. The achieved RMSE evaluated on the QZ sphere volume is 0.0120, and we have a value of $E_{MAX} = 15.4$dB (calculated on the plane parallel to the PWG plane and passing through the center of the sphere). It is worth mentioning that the number of radiating elements is almost the same as the solution proposed in [17] (where the authors employed 172 radiators). The authors of the comparing paper do not provide the RMSE for that solution, but only the maximum oscillation of the amplitude and phase on the $(y, z)-$plane within the sphere, which are equal to ± 0.5dB and $\pm 10°$(deg), respectively [18]. Our solution achieves a maximum oscillation of the amplitude and phase of the field on the same plane of ± 0.35dB and $\pm 2.9°$(deg), values significantly better than the comparing solution.

C. Full wave validation

As a final confirmation of the synthesis approach, we have validated the proposed synthesis approach using a full wave simulation. To perform the full-wave calculations in a reasonable time using the available hardware, we have considered a smaller QZ with respect to previous examples. In particular, we have required a circular QZ of a radius of $\rho_{MAX} = 2.5\lambda$ at a distance of $z = 5\lambda$ from the PWG plane.

By using the proposed ring-synthesis approach, using a set of equispaced rings in the range $(1\lambda; 4\lambda)$ and $\epsilon_A = \epsilon_B = \epsilon_C = 0.01$ we can obtain a set of $N = 4$ rings. The calculation of these rings required 11 iterations in a total time of less than one minute.

Once we have calculated the ring radii, we can obtain the number of discrete sources M_n for the $n-$th ring by selecting the lowest number of sources that guarantees $\sigma_A < 10^{-4}$. Once the values of M_n have been calculated, we can compute the actual excitation of the radiators belonging to these rings. All the parameters of the PWG that account for an

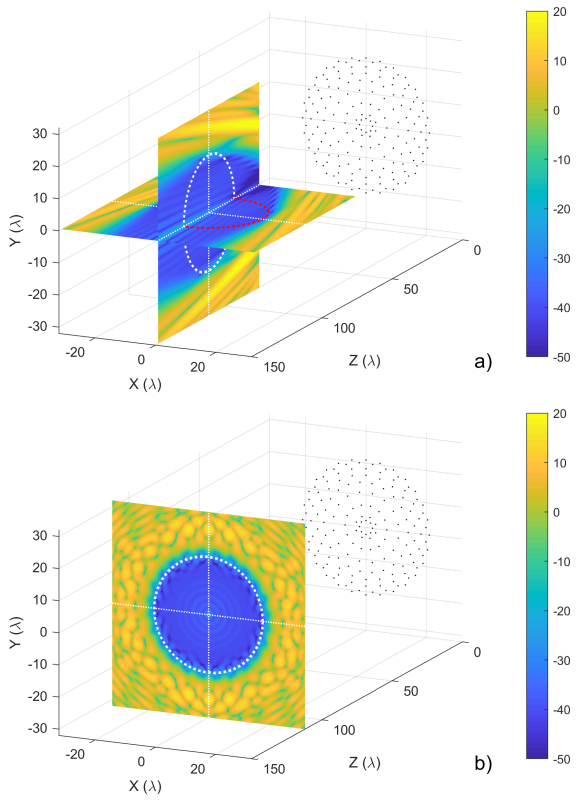

Fig. 7. Difference $\Delta E(x, y, z)$ of the field radiated by the 170 elements PWG and the wanted plane wave: a) the difference is calculated on the $x = 0$ and $y = 0$ planes; b) the difference is calculated on the $z = 112\lambda$ plane. A dashed white line shows the sphere of radius ρ_{MAX}; the red dotted arc is the meridian arc employed for the synthesis.

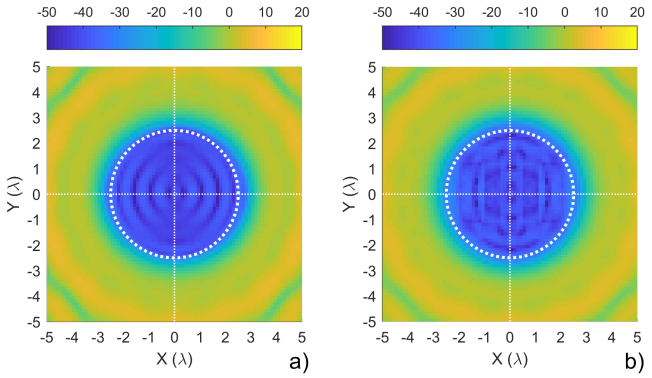

Fig. 8. Difference $\Delta E(x, y, z)$ of the field radiated by the 52 elements PWG and the wanted plane wave on the $z = 5\lambda$ plane: a) PWG made by $y-$polarized elementary sources; b) PWG made by rectangular patch elements. A dashed white line is used to show the circle of radius ρ_{MAX}.

overall number of 54 $y-$oriented linearly polarized elementary sources are in table III.

In Fig.8a, it is possible to see the plot of the difference between the field radiated by the PWG made of $y-$polarized elementary sources and the wanted plane wave. The difference between the field radiated by the PWG and the desired plane wave is very small in the circle of radius 2.5λ. The achieved RMSE is 0.0099 and a value of $E_{MAX} = 0.65$dB.

Using the achieved radiators' coordinates and excitations,

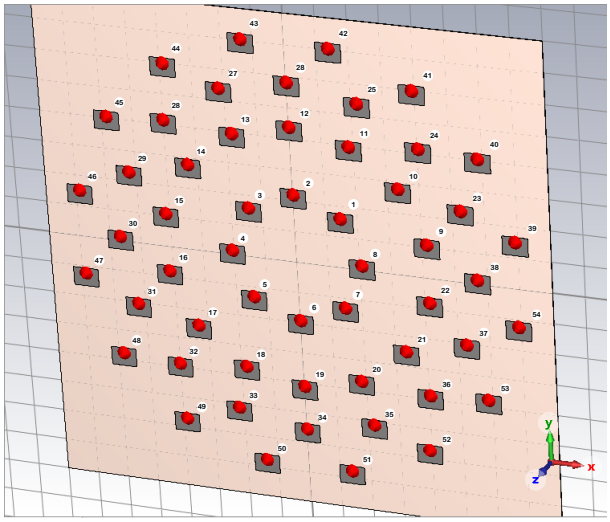

Fig. 9. Layout of the PWG made of 54 patch antennas working at the frequency of 3GHz.

we have simulated, at the frequency of 3GHz, an array of 54 rectangular patch elements of 40×29.6mm, built on a 1mm thick substrate of Arlon AD250C having a square side of 800mm with the same relative excitations calculated for the linearly polarized elementary sources. The patch elements are excited by 50Ω lumped ports having a distance of 5.9mm from the center of the patch to resonate at the frequency of 3GHz and to obtain a linearly polarized field in the broadside direction. A plot of the simulated PWG array is provided in Fig.9.

In Fig.6b, it is possible to see the plot of the difference between the field radiated by the patch element PWG and the wanted plane wave. The difference between the field radiated by the PWG employing patch antennas and the desired plane wave is small: the achieved RMSE is 0.0131 and a value of $E_{MAX} = 0.26$dB.

The substitution of the elementary source with the patch antenna has only marginally modified the overall quality of the synthesized QZ. Using a different type of radiating elements (with a stronger mutual coupling or a more directive pattern), it may be possible that the quality of the approximation in the quiet zone may become unacceptable; in this case, it is possible to use the measurement or simulation of the active element pattern, together with convex programming techniques, to correct the excitations of the radiating elements slightly.

V. Conclusions

We have presented a method for the efficient and effective design of PWGs. The approach is based on using convenient circularly polarized ring sources, which reduce the computational complexity of the synthesis problem, which becomes similar to sparse linear array synthesis. These particular sources are used only as a device to simplify the design process, since the final PWG can employ common linearly polarized feeds.

The examples shown confirm the quality of the approach, which can provide better overall performance with respect to

concurrent algorithms or a significant reduction in the number of radiators needed. We have also verified the technique's applicability to realistic radiators through the full-wave simulation of a patch antenna array used as PWG.

In future developments, we plan to work on synthesizing isophoric PWG so that all the radiating elements can be excited with the same signal amplitude; we also plan on working on the maximization of the power transferred to the QZ, as well as including mutual coupling in the synthesis and implementing more directive feeds.

APPENDIX

We will now provide some insights into the field radiated by the CPES.

With reference to (1), we can notice only the term $\mathbf{D} = ((\mathbf{i}_y + j\mathbf{i}_x) \times \mathbf{i}_{R_0}) \times \mathbf{i}_{R_0}$ depends from θ. With some simple algebra calculations, we can obtain its explicit form:

$$\mathbf{D} = D_x\mathbf{i}_x + D_y\mathbf{i}_y + D_z\mathbf{i}_z \tag{26}$$

with

$$D_x{=}(\rho^2\cos\theta\sin\theta - jz^2 - j\rho^2\sin^2\theta)/(\rho^2+z^2) \tag{27}$$
$$D_y{=}(-\rho^2\cos^2\theta - z^2 + j\rho^2\cos\theta\sin\theta)/(\rho^2+z^2) \tag{28}$$
$$D_z{=}(j\rho z e^{-j\theta})/(\rho^2+z^2) \tag{29}$$

Remembering that $\mathbf{i}_y = (\mathbf{i}_r + \mathbf{i}_\ell)/2$ and $\mathbf{i}_x = (\mathbf{i}_r - \mathbf{i}_\ell)/(2j)$ and substituting these relationships into (26), we can obtain

$$\mathbf{D} = \frac{-z^2 - \rho^2/2}{\rho^2+z^2}\mathbf{i}_r + \frac{-\rho^2 e^{-2j\theta}/2}{\rho^2+z^2}\mathbf{i}_\ell + \frac{j\rho z e^{-j\theta}}{\rho^2+z^2}\mathbf{i}_z \tag{30}$$

thus demonstrating that in (2) the RH polarized term is independent from θ, the LH polarized term contains a factor $e^{-2j\theta}$, and the z component contains a factor $e^{-j\theta}$.

A representation of the three complex scalar functions $A_0(\rho,z)$, $B_0(\rho,z)$ and $C_0(\rho,z)$ appearing in (2) on the observation plane is given in Fig.10.

We obtain a behavior similar to (2) when considering an LH-CPES, whose field is:

$$\tilde{\mathbf{E}_\mathbf{0}}^{(l)}(\rho,\theta,z) = A_0(\rho,z)\mathbf{i}_\ell + B_0(\rho,z)e^{+j2\theta}\mathbf{i}_r + C_0(\rho,z)e^{+j\theta}\mathbf{i}_z. \tag{31}$$

Let us now analyze the field radiated by a CPCRS.

With reference to Fig.11a, let us consider the field $\mathbf{E}_1$ radiated by an RH-CPCRS of radius q in the point P_1 of coordinates $(\rho, \theta = 0, z)$. This field can be decomposed into its Cartesian coordinates as:

$$\begin{aligned}\mathbf{E}_1 &= \mathbf{E}^{(r)}(\rho,\theta=0,z,q)\\ &= E_x(\rho,z,q)\mathbf{i}_x + E_y(\rho,z,q)\mathbf{i}_y + E_z(\rho,z,q)\mathbf{i}_z\end{aligned} \tag{32}$$

Let us now imagine performing a geometrical rotation of the RH-CPCRS and the observation plane of an angle θ, as in Fig.11b, so that we can define a new (u,v,z) coordinate system:

$$\mathbf{u} = \cos\theta\mathbf{i}_x + \sin\theta\mathbf{i}_y \quad \text{and} \quad \mathbf{v} = \cos\theta\mathbf{i}_y - \sin\theta\mathbf{i}_x \tag{33}$$

The new position of the point P_1 will be marked as P_2, and the value of the field $\mathbf{E}_2$ in that point will be

$$\mathbf{E}_2 = E_x\mathbf{i}_u + E_y\mathbf{i}_v + E_z\mathbf{i}_z \tag{34}$$

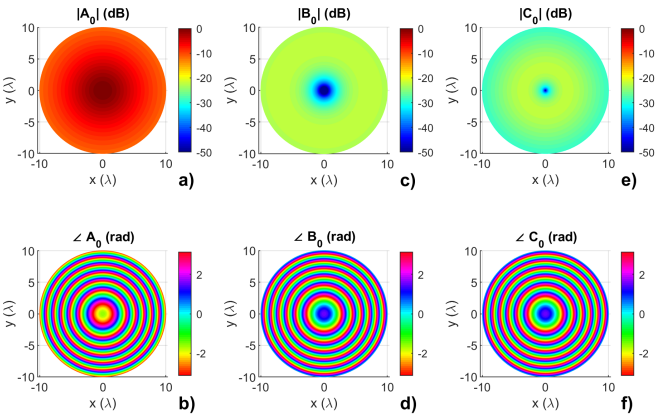

Fig. 10. Representation of the field radiated by an RH-CPES on an observation plane with $z = 5\lambda$ using the complex functions A_0, B_0, and C_0. Subplots a)-c)-e) provide the amplitude of the functions; subplots b)-d)-f) provide the phases. The amplitudes are normalized to the maximum amplitude of A_0.

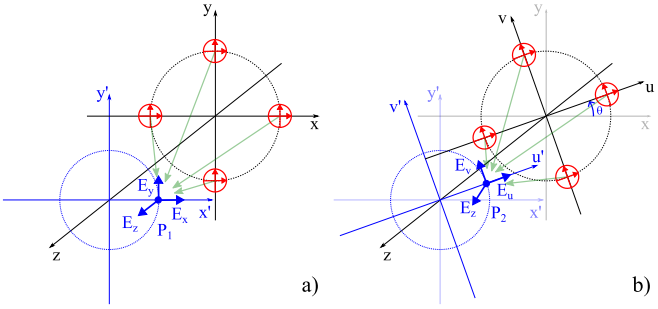

Fig. 11. Scheme of the representation of the fields in the rotated coordinate system; only four CPES of the CPCRS are depicted for simplicity. Subplot a): standard system; subplot b): rotated system.

where the dependence of the complex functions E_x, E_y and E_z, from the variables (ρ,z,q) will be dropped for easiness of notation.

Since we are dealing with a CPCRS, it is easy to recognize that the original ring source of Fig.11a is perfectly identical to the rotated one, except for a phase factor $e^{-j\theta}$, that takes into account the rotation of the individual CPESs that constitute the CPCRS.

According to this observation, we can calculate the field in the point of coordinates (ρ,θ,z) as:

$$\mathbf{E}^{(r)}(\rho,\theta,z,q) = (E_x\mathbf{u} + E_y\mathbf{v} + E_z\mathbf{i}_z)\,e^{-j\theta} \tag{35}$$

We can now substitute the complex amplitudes $\mathbf{E}_x$ and $\mathbf{E}_y$ with a proper summation of a right-handed circularly polarized component E_r and a left-handed circularly polarized component E_ℓ; remembering the following relationships

$$\begin{aligned}E_r\mathbf{i}_r + E_\ell\mathbf{i}_\ell &= E_r(\mathbf{i}_y + j\mathbf{i}_x) + E_\ell(\mathbf{i}_y - j\mathbf{i}_x) =\\ &= j(E_r - E_\ell)\mathbf{i}_x + (E_r - E_\ell)\mathbf{i}_y = E_x\mathbf{i}_x + E_y\mathbf{i}_y\end{aligned} \tag{36}$$

we can obtain:

$$\mathbf{E}^{(r)}(\theta) = (j(E_r - E_\ell)\mathbf{u} + (E_r + E_\ell)\mathbf{v} + E_z\mathbf{i}_\mathbf{z})\,e^{-j\theta} \tag{37}$$

Substituting (33) into (37), with some simple algebraic manipulations we find:

$$\mathbf{E}^{(r)}(\theta) = E_r \mathbf{i}_r + E_\ell \mathbf{i}_\ell e^{-j2\theta} + E_z \mathbf{i}_\mathbf{z} e^{-j\theta} \tag{38}$$

The last equation demonstrates (7) since it shows that the right-handed circularly polarized component of the field $\mathbf{E}^{(r)}$ is independent of the angular coordinate θ, while its left-handed component and its z-component show a phase variation proportional to -2θ and $-\theta$, respectively.

ACKNOWLEDGMENTS

This paper has been supported in part by the MIUR program "Dipartimenti di Eccellenza 2018-2022".

REFERENCES

[1] G. E. Evans, "Antenna measurement techniques," *Norwood*, 1990.

[2] R. Haupt, "Generating a plane wave with a linear array of line sources," *IEEE Trans. Antennas Propag.*, vol. 51, no. 2, pp. 273–278, 2003.

[3] O. M. Bucci, M. D. Migliore, G. Panariello, and D. Pinchera, "Plane-wave generators: Design guidelines, achievable performances and effective synthesis," *IEEE Trans. Antennas Propag.*, vol. 61, no. 4, pp. 2005–2018, 2012.

[4] C. Rowell and A. Tankielun, "Plane wave converter for 5g massive mimo basestation measurements," in *12th Europ. Conf. on Antennas and Prop. (EuCAP)*. IET, 2018, pp. 1–3.

[5] Y. Zhang, Z. Wang, X. Sun, Z. Qiao, W. Fan, and J. Miao, "Design and implementation of a wideband dual-polarized plane wave generator with tapered feeding nonuniform array," *IEEE Antennas Wireless Propag. Lett.*, vol. 19, no. 11, pp. 1988–1992, 2020.

[6] S. Catteau, M. Ivashina, and R. Rehammar, "Design and simulation of a 28 ghz plane wave generator for nr measurements," in *14th Europ. Conf. on Antennas and Prop. (EuCAP)*. IEEE, 2020, pp. 1–4.

[7] Z. Yang, Z. Wang, Y. Zhang, and S. Gao, "Robust plane wave generator design in small anechoic chamber setup using parameterized field method," *IEEE Access*, vol. 8, pp. 187 052–187 059, 2020.

[8] R. Maaskant, O. A. Iupikov, P. S. Krasov, R. Rehammar, A. A. Glazunov, and M. V. Ivashina, "A new hybrid chamber for generating a spectrum of oblique incident plane waves at the dut," *IEEE Trans. Antennas Propag.*, vol. 69, no. 10, pp. 6806–6815, 2021.

[9] D. Pinchera and M. D. Migliore, "A novel approach for circular array testing," in *11th Europ. Conf. on Antennas and Prop. (EUCAP)*. IEEE, 2017, pp. 1457–1460.

[10] Y. Li, L. Gao, H. Sun, and X. Zhang, "Plane-wave synthesis: A sparse representation perspective," *IEEE Antennas Wireless Propag. Lett.*, vol. 19, no. 9, pp. 1644–1648, 2020.

[11] G. Franceschetti, *Electromagnetics: theory, techniques, and engineering paradigms*. Springer Science & Business Media, 2013.

[12] E. J. Candes, M. B. Wakin, and S. P. Boyd, "Enhancing sparsity by reweighted l1 minimization," *Journal of Fourier anal. and appl.*, vol. 14, no. 5, pp. 877–905, 2008.

[13] D. Pinchera, M. D. Migliore, F. Schettino, M. Lucido, and G. Panariello, "An effective compressed-sensing inspired deterministic algorithm for sparse array synthesis," *IEEE Trans. Antennas Propag.*, vol. 66, no. 1, pp. 149–159, 2018.

[14] D. Pinchera, M. D. Migliore, and G. Panariello, "Isophoric inflating deflating exploration algorithm (i-idea) for equal-amplitude aperiodic arrays," *IEEE Transactions on Antennas and Propagation*, vol. 70, no. 11, pp. 10 405–10 416, 2022.

[15] O. M. Bucci, T. Isernia, S. Perna, and D. Pinchera, "Isophoric sparse arrays ensuring global coverage in satellite communications," *IEEE Trans. Antennas Propag.*, vol. 62, no. 4, pp. 1607–1618, 2013.

[16] M. Grant and S. Boyd, "CVX: Matlab software for disciplined convex programming, version 2.1," http://cvxr.com/cvx, Mar. 2014.

[17] F. Scattone, D. Sekuljica, A. Giacomini, F. Saccardi, A. Scannavini, E. Kaverine, S. Anwar, N. Gross, P. O. Iversen, and L. J. Foged, "Preliminary assesment of millimeter wave plane wave generator for 5g device testing," in *15th Europ. Conf. on Antennas and Prop. (EuCAP)*, 2021, pp. 1–5.

[18] F. Scattone, D. Sekuljica, A. Giacomini, F. Saccardi, R. T. Sánchez, A. Scannavini, K. Rutkowski, E. Kaverine, S. Anwar, N. Gross *et al.*, "Production measurement of 5g millimeter wave plane wave generators," in *16th Europ. Conf. on Antennas and Prop. (EuCAP)*. IEEE, 2022, pp. 1–3.